Hydrometeorological Factors Controlling the Stable Isotopic Composition of Precipitation in the Highlands of South Ecuador

DARÍO X. ZHIÑA,[a] GIOVANNY M. MOSQUERA,[b,a] GERMAIN ESQUIVEL-HERNÁNDEZ,[c] MARIO CÓRDOVA,[a] RICARDO SÁNCHEZ-MURILLO,[d] JOHANNA ORELLANA-ALVEAR,[a,e] AND PATRICIO CRESPO[a]

[a] *Departamento de Recursos Hídricos y Ciencias Ambientales and Facultad de Ingeniería, Universidad de Cuenca, Cuenca, Ecuador*
[b] *Instituto Biósfera, Universidad San Francisco de Quito USFQ, Quito, Ecuador*
[c] *Stable Isotopes Research Group and Water Resources Management Laboratory, Chemistry Department, Universidad Nacional, Heredia, Costa Rica*
[d] *Department of Earth and Environmental Sciences, The University of Texas at Arlington, Arlington, Texas*
[e] *Laboratory for Climatology and Remote Sensing, Faculty of Geography, University of Marburg, Marburg, Germany*

(Manuscript received 12 September 2021, in final form 10 April 2022)

ABSTRACT: Knowledge about precipitation generation remains limited in the tropical Andes due to the lack of water stable isotope (WSI) data. Therefore, we investigated the key factors controlling the isotopic composition of precipitation in the Páramo highlands of southern Ecuador using event-based (high frequency) WSI data collected between November 2017 and October 2018. Our results show that air masses reach the study site preferentially from the eastern flank of the Andes through the Amazon basin (73.2%), the Orinoco plains (11.2%), and the Mato Grosso Massif (2.7%), whereas only a small proportion stems from the Pacific Ocean (12.9%). A combination of local and regional factors influences the $\delta^{18}O$ isotopic composition of precipitation. Regional atmospheric features (Atlantic moisture, evapotranspiration over the Amazon rainforest, continental rain-out, and altitudinal lapse rates) are what largely control the meteoric $\delta^{18}O$ composition. Local precipitation, temperature, and the fraction of precipitation corresponding to moderate to heavy rainfalls are also key features influencing isotopic ratios, highlighting the importance of localized convective precipitation at the study site. Contrary to $\delta^{18}O$, *d*-excess values showed little temporal variation and could not be statistically linked to regional or local hydrometeorological features. The latter reveals that large amounts of recycled moisture from the Amazon basin contribute to local precipitation regardless of season and predominant trajectories from the east. Our findings will help to improve isotope-based climatic models and enhance paleoclimate reconstructions in the southern Ecuador highlands.

KEYWORDS: Atmosphere; South America; Tropics; Convection; Precipitation; Rainfall; Isotopic analysis; Regression analysis; Mountain meteorology; Regional effects

1. Introduction

Understanding precipitation formation and the key factors influencing it in complex mountainous regions is important because these regions supply the water needs of millions of people, particularly in light of changes in climate (Ingraham 1998; Sloat et al. 2018; Thibeault et al. 2012; Sánchez-Murillo et al. 2020). This knowledge is also of great need for improving and validating climate models, predicting precipitation at local and regional scale, and assessing how future changes in climate will affect the water balance of catchments. Obtaining this information is important to help identify effective and economic measures to counteract future changes in precipitation patterns. In response to this, current hydrometeorological research aims at identifying the origin and pathways of water vapor masses and the factors influencing the formation of precipitation (Gimeno 2013). However, this knowledge remains limited for the highlands of the tropical Andes, extending from western Venezuela to northern Peru.

Analysis of the stable isotopic composition of hydrogen and oxygen in precipitation—expressed as δ^2H and $\delta^{18}O$, respectively—has become one of the most powerful methodologies to underpin precipitation formation (Araguás-Araguás et al. 2000; He et al. 2018; Kaseke et al. 2018). These tracers provide information about the history of water forming local precipitation. This is partially possible through the comparison of the global relation between δ^2H and $\delta^{18}O$ in precipitation, known as the global meteoric water line (GMWL) defined by the linear relationship: $\delta^2H = 8\delta^{18}O + 10‰$, and the local meteoric water line (LMWL) derived from the relation between both isotopes in precipitation collected at a specific site (Craig 1961). Differences in slope and intercept between the LMWL relative to the GMWL provides information about the source of moisture, e.g., continental versus maritime, moisture recycling, regional re-evaporation processes, and/or atmospheric conditions under which local precipitation is formed (Kendall and McDonnell 1999; Leibundgut et al. 2009). Additional information can be obtained through the analysis of the temporal variability of δ^2H, $\delta^{18}O$, and deuterium excess (hereafter referred to as *d*-excess $= \delta^2H - 8\delta^{18}O$) (Dansgaard 1964), and their relationship with in situ atmospheric conditions, e.g., relative

Supplemental information related to this paper is available at the Journals Online website: https://doi.org/10.1175/JHM-D-21-0180.s1.

Corresponding author: Giovanny M. Mosquera, giovamosquera@gmail.com, gmosquera@usfq.edu.ec

DOI: 10.1175/JHM-D-21-0180.1

humidity, air temperature, wind speed and direction, radiation, precipitation type, and amount. Moreover, since regional atmospheric features may also play an important role in precipitation formation processes, water stable isotopes (WSIs) are often used in combination with complementary methods that provide information about regional meteorological conditions affecting the trajectory of water vapor masses.

A variety of air mass transport models are currently used to determine the pathways of air masses from their origin to where they condensate and precipitate. Among them are the widely used Lagrangian transport models (e.g., Ciric et al. 2016; Heydarizad et al. 2019; Le Duy et al. 2018; Sánchez-Murillo et al. 2017). In hydrometeorological and climatological studies, these types of models helped to determine the main sources of humidity contributing to local precipitation at a given site, as well as their trajectory (Heydarizad et al. 2019). Lagrangian models also provide information about the "regional" meteorological conditions air masses undergo along their pathway and the factors that affect the formation of local precipitation. Lagrangian transport models in combination with WSI data collected at different temporal resolutions have been used in different tropical regions including Central America and Southeast Asia (e.g., Le Duy et al. 2018; Sánchez-Murillo et al. 2016, 2017). Although weekly or monthly WSI data are helpful to provide insights into moisture sources contributing to local precipitation, data collected at high temporal frequency, e.g., subdaily or during rainstorm events, during at least a complete hydrological year are needed to obtain a thorough understanding of the local and/or regional factors influencing the isotopic composition of precipitation. The latter allows identifying how contributions from different vapor sources influence the formation of precipitation.

To our knowledge, there are only two studies in the tropical Andes that used the combined WSI–air mass transport model approach. Windhorst et al. (2013) used isotopic data collected at a high temporal frequency (rainstorm events) over a short period (September–December 2010) to investigate how elevation and local climate variables influence the isotopic composition of precipitation at a tropical forest site situated between 1800 and 2800 m MSL. The short study period limited these authors from providing a complete understanding of how their findings were representative over a complete hydrological year. Differently, Esquivel-Hernández et al. (2019) used a dataset collected in 17 months (January 2015–May 2016) at a weekly time scale in the tropical alpine highlands (3900 m MSL) of south Ecuador. Although this study preliminarily identified the sources of moisture contributing to local precipitation, the coarse temporal resolution of the used data prevented the study from distinguishing among individual storm origins and trajectories (continental versus maritime and/or Amazon rainforest versus Pacific Ocean) because water from individual storms mixed in the bulk weekly samples. It is important to note that until now the potential effect of regional climatic factors on the isotopic composition of precipitation in the study region has not been assessed.

Through the combined analysis of WSI data collected at high temporal frequency (during rainstorm events) and the use of Lagrangian transport models, this study aims to address the following research questions:

1) What are the main pathways of air masses that form local precipitation in the tropical alpine highlands of southern Ecuador?
2) What are the main meteorological factors, in situ and/or at the regional level, that influence the isotopic composition of precipitation at the study region?

2. Materials and methods

a. Study site

The study site, the Zhurucay Ecohydrological Observatory (ZEO, Fig. 1), is located in the Páramo ecosystem in southern Ecuador between 3400 and 3900 m MSL (Mosquera et al. 2015). The climate of the study area is mainly influenced by continental air masses originating from the Amazon basin on the east; and to a lesser extent by water vapor from the Pacific Ocean (Esquivel-Hernández et al. 2019; Vuille et al. 2000). Mean temperature and mean annual precipitation estimated in the period 2011–14 are 6.0°C (Córdova et al. 2015) and 1345 mm at 3780 m MSL (Padrón et al. 2015). Precipitation is uniformly distributed throughout the year, presenting a less wet period in August and September. Precipitation intensity is low, rarely exceeding 5 mm h^{-1} and falling primarily as drizzle (Padrón et al. 2015). The mean duration of precipitation events at the study site is 225 min (Orellana-Alvear et al. 2017). The isotopic composition of precipitation is variable showing a seasonal pattern. Low/depleted values are observed during the most humid periods (April–May) and high/enriched values during the less wet months (August–September). The linear regression (type II) between δ^2H and δ^{18}O using 212 precipitation samples collected during the period May 2011–May 2013 presents a slope of 8.37 ± 0.04 and an intercept of 18.04 ± 0.39‰ (Mosquera et al. 2016a,b).

b. Meteorological data collection

An automatic weather station located at the upper part of the ZEO (3°03′44.6″S, 79°14′05.8″W; 3780 m MSL), hereafter referred to as the ZEO Super Site (Fig. 1), consisted of a Campbell Scientific CS-215 probe for measuring temperature and relative humidity, a Met-One 034B Windset anemometer, an Apogee CS300 pyranometer, and a Texas TR-525M tipping-bucket rain gauge with a resolution of 0.1 mm. These variables were recorded every 5 min during the study period, i.e., from 1 November 2017 to 31 October 2018. These data were used as "in situ factors" that could influence the temporal variability of the isotopic composition of precipitation.

The fractions of different types of rainfall in the study area were determined with a disdrometer (Thies Clima 2007) located at the Super Site (Fig. 1). This is a laser sensor that produces a horizontal light beam whose signal is attenuated by precipitation particles. The diameter of the raindrops (D) is estimated from the reduction in amplitude of the attenuated

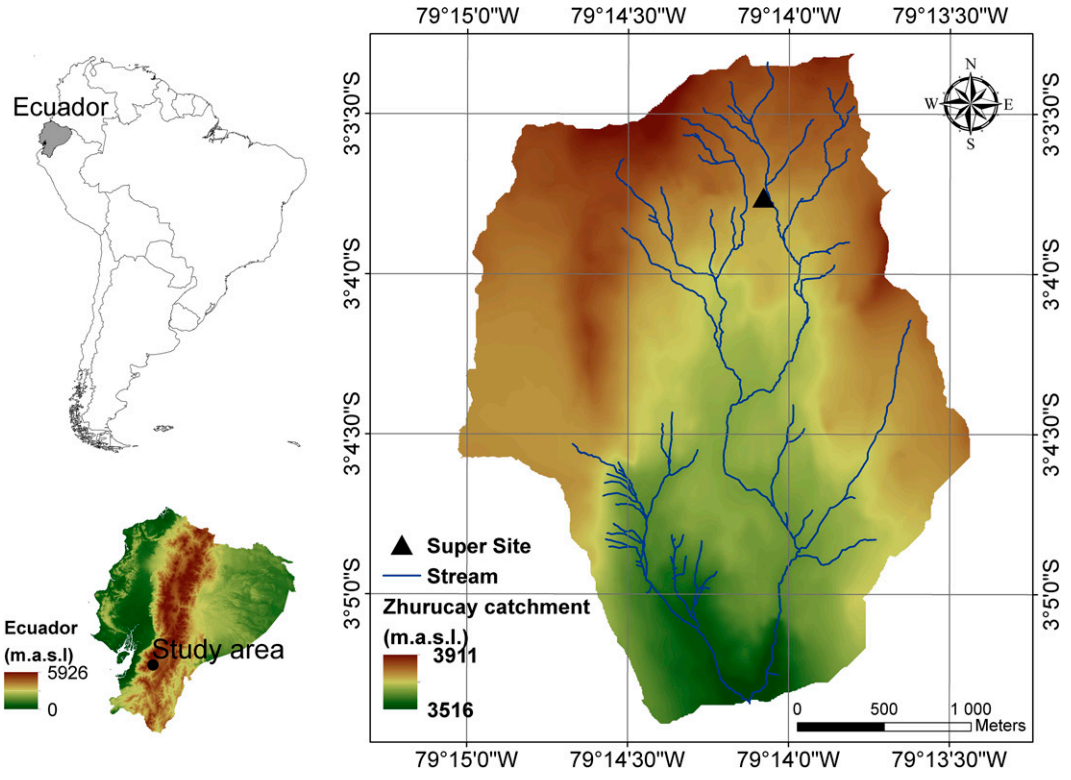

FIG. 1. The Zhurucay Ecohydrological Observatory (ZEO) situated in southern Ecuador. The black triangle in the map shows the location of the Super Site where the sequential sampler for collecting rainwater samples at high temporal frequency (3°03′44.6″S, 79°14′05.8″W; 3780 m MSL), the meteorological station, and the laser disdrometer were installed.

signal. The disdrometer operates at a wavelength of 785 nm and has a reference measurement area of 45.6 cm^2 and a resolution of 0.005 mm h^{-1}. Disdrometer data were also recorded every 5 min. The methodology described by Orellana-Alvear et al. (2017) was followed to classify the type of precipitation and their fractions during different periods of interest. The mean volume diameter (D_m) was used to characterize the drop size distribution at each time step. In this way each rainfall observation was classified as light (0.1 mm $< D_m \leq$ 0.5 mm), moderate (0.5 mm $< D_m \leq$ 1.0 mm), heavy (1.0 mm $< D_m \leq$ 2.0 mm), and very heavy ($D_m >$ 2 mm). Their respective contributions (percentages) to each of the collected precipitation samples for isotope analysis were estimated. The calculated fractions of each rainfall type were also evaluated as potential local factors influencing the stable isotopic composition of precipitation.

c. *Isotopic data collection and laboratory analysis*

Precipitation samples for stable isotopes analysis were collected during rainfall events at the ZEO Super Site (Fig. 1) in the period 1 November 2017–31 October 2018 (n = 295). Sampling was carried out using a handmade sequential rainfall sampler. The principle of operation of the sequential rainfall sampler is pressure based, whereby precipitation water fills a bottle until a certain pressure is reached (i.e., atmospheric pressure). At this stage, water is diverted to another bottle and in this way, it is possible to obtain sequential samples of an entire precipitation event (McDonnell 1990). Each bottle collects 160 mL of water, corresponding to a 2.08-mm rainfall depth. Precipitation data from a rain gauge located 3 m from the sequential sampler were used to determine the time at which each bottle was filled with water. Precipitation was collected and stored in 2-mL amber glass vials. The use of a thin layer of mineral oil in the rainfall collector is recommended to avoid fractionation by evaporation (Mook and Rozanski 2000). However, this was not applied in this study because evaporation did not affect the water samples, as verified during a test period of the sequential sampler 3 months before the start of this study. All samples collected during the test period were plotted in the δ^2H–$\delta^{18}O$ dual space and compared to the historical LMWL (2011–18) of the study site, showing that evaporation did not affect their isotopic composition. The collected samples were covered with parafilm and shielded from the sunlight to prevent fractionation by evaporation during transport and storage until their analysis in the laboratory (IAEA 2014; Mook and Rozanski 2000).

The isotopic composition of the precipitation samples was measured at the Water Quality Laboratory of the Department of Water Resources and Environmental Sciences of the University of Cuenca using a cavity ring-down spectrometer L1102-*i* Picarro (Picarro Inc., United States). The Picarro

secondary reference standards were ZERO (δ^2H = 0.3 ± 0.2‰, δ^{18}O = 1.8 ± 0.9‰), MID (δ^2H = −20.6 ± 0.2‰, δ^{18}O = −159.0 ± 1.3‰), and DEPL (δ^2H = −29.3 ± 0.2 ‰, δ^{18}O = −235.0 ± 1.8‰). We applied six sample injections and discarded the first three as recommended by the manufacturer to minimize memory effects (Penna et al. 2012). For the last three injections, we calculated the maximum δ^{18}O and δ^2H differences and compared them with the analytical precision given by the manufacturer and the standard deviation of the isotopic standards used for the analyses. Samples that showed measurement differences larger than the latter were reanalyzed. We used three standards every fifteen samples for the analyses. ZERO and DEPL standards were used to normalize the results to the VSMOW-SLAP (Vienna Standard Mean Ocean Water–Standard Light Antarctic Precipitation) scale, while MID was used as a quality control and drift control standard. The ^{18}O/^{16}O and ^{2}H/^{1}H ratios are presented in delta notation δ (‰, per mil), relative to the VSMOW-SLAP scale. The long-term instrument precision is 0.5‰ for hydrogen (δ^2H) and 0.1‰ for oxygen (δ^{18}O). Organic contamination of the isotopic composition was verified with the ChemCorrect 1.2.0 software (Picarro 2010), no samples were contaminated.

d. Origin and trajectories of water vapor masses

The origin and trajectory of water vapor masses were determined through the generation of backward trajectories based on the Hybrid Single-Particle Lagrangian Integrated Trajectory (HYSPLIT) model (Draxler and Hess 1998; Stein et al. 2015). The HYSPLIT model determines the position of water vapor masses using a three-dimensional Lagrangian velocity algorithm of air masses (Stein et al. 2015). The input data needed by the HYSPLIT model correspond to the variables of pressure, temperature, wind speed, and solar radiation obtained from the NOAA meteorological database (GDAS, global data assimilation system: from 2006 to present; 0.5° resolution; Rolph et al. 2017; Su et al. 2015). For each collected precipitation sample (n = 295) a backward trajectory was reconstructed for a period of 192 h (8 days) with a 1-h interval. The calculation time was selected according to the expected residence time of water in the atmosphere, i.e., 4–10 days (Van Der Ent and Tuinenburg 2017). In addition, a height of 3800 m MSL (633 hPa) was chosen for the start of the backward trajectory, because this height most probably corresponds to the height of the cloud base (Esquivel-Hernández et al. 2019; Lawrence 2005). The HYSPLIT model provides information about the variables that influence the determined air moisture trajectories. These variables, which are considered potential "regional" factors influencing the isotopic composition of precipitation, include potential temperature, air temperature, precipitation rate, relative humidity, solar radiation, pressure, mix depth (the vertical distance between the ground surface and the altitude at which chemical substances mix), and altitude of the air parcel.

Trajectories of the air masses were analyzed based on the regions considered as sources of atmospheric humidity through which they traveled before reaching the study area. These regions were defined based on the study of Agudelo et al. (2018). The sources of atmospheric humidity included 17 regions (as shown in Fig. 2): 5 oceanic and 12 continental regions.

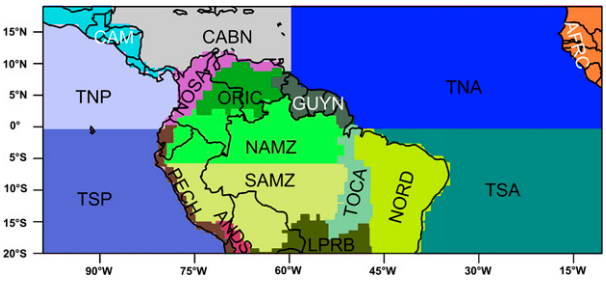

FIG. 2. Regions considered as sources of moisture through which the air masses travel before reaching the study area. The 17 regions correspond to Central America (CAM), northern South America (NOSA), Orinoco basin (ORIC), Guyanas (GUYN), Peru–Chile (PECH), Northern Amazon (NAMZ), Southern Amazon (SAMZ), subtropical Andes (ANDS), Tocantins basin (TOCA), La Plata River basin (LPRB), Brazil's Northeast (NORD), Africa (AFRC), tropical North Pacific (TNP), tropical South Pacific (TSP), Caribbean Sea (CABN), tropical North Atlantic (TNA), and tropical South Atlantic (TSA). Figure adapted from Ruiz-Vásquez et al. (2020).

e. LMWL and d-excess analysis

This analysis was carried out by comparing the slopes and intersections of the LMWL of the study site with the GMWL. Comparison of both lines permits to identify if re-evaporation processes affect local precipitation (Noone 2012; Putman et al. 2019). The construction of the LMWL was carried out through linear regression of the isotopic composition of δ^{18}O and δ^2H from precipitation samples and their adjustment was assessed using the coefficient of determination (R^2). Also, an analysis of d-excess was conducted to identify moisture recycling processes caused by the transpiration of plants and the evaporation of water from surfaces and water bodies. High values of d-excess indicate that local precipitation was composed of recycled moisture (Froehlich et al. 2008; Pang et al. 2011; Salati et al. 1979).

f. Analysis of factors controlling the isotopic composition of precipitation

Given that the stable isotopic composition of precipitation at a given site depends on the origin and transport of atmospheric moisture, as well as in situ meteorological conditions, the analysis was carried out using precipitation isotopic composition (δ^{18}O, δ^2H, and d-excess) and local and regional meteorological variables. Local factors encompassed the meteorological variables measured at the ZEO Super Site climate station (Fig. 1). These variables included accumulated precipitation (Prec_i), average temperature (Temp_i), average relative humidity (RH_i), average wind speed (WS_i), average atmospheric pressure (Press_i), and average solar radiation (SR_i) aggregated for the sampling period corresponding to

each of the collected precipitation samples for isotope analysis. The subscript "*i*" after each of the variables indicates they were measured in situ. Also, the fractions of different rainfall types based on the diameter of the raindrops occurring in the study area were considered as possible controlling factors. That is, light (L), moderate (M), heavy (H), and very heavy (VH) rainfall, and several combinations among those fractions:

L + M, M + H, H + VH, L + M + H, and M + H + VH.

Regional factors included the meteorological conditions along the trajectory of the water vapor masses generated by the HYSPLIT model. The outputs from the model (i.e., trajectory-integrated meteorological fields, hereafter referred to as "regional variables") correspond to rainfall rate along the trajectory (Prec_x), trajectory altitude (Alt_x), air temperature (Temp_x), potential temperature (PT_x), mix depth (MD_x), pressure (Press_x), downward solar radiation flux (SR_x), and relative humidity (RH_x). As the model produces hourly outputs along the determined air mass trajectories, daily averages from 1–8 days backward (the subscript x after each of the regional variables indicates the corresponding backward day) were used to investigate the influence of these regional variables on the isotopic composition of local precipitation.

The analysis of the factors influencing the isotopic composition of precipitation comprised a series of steps. First, a multicollinearity analysis among the in situ and regional variables was performed to remove redundant information that may affect the statistical analyses. The criteria used for this purpose was the variance factor index (VIF) (Lin et al. 2011) considering a threshold value of 3 (Hair et al. 2016). Subsequently, Spearman's correlation analysis was performed using the variables yielded from the VIF analysis and the values of the isotopic composition of precipitation. If high correlation values were obtained ($r \geq 0.7$), simple linear regression (SLR) models were developed between these variables and the isotopic composition of precipitation. Variables producing $R^2 \geq 0.5$ were considered as drivers of the isotopic composition of precipitation (Van Liew et al. 2003; Moriasi et al. 2007; Santhi et al. 2001). If low correlation values ($r < 0.7$) were obtained, the next step was to apply multiple linear regression models (MLRs) between meteorological variables (local and regional) and the isotopic composition of precipitation. The MLRs were built using bidirectional stepwise criteria (Helsel and Hirsch 2002; Wang et al. 2013) permitting the inclusion of variables in the MLRs using the forward stepwise criteria and discarded using the backward stepwise criteria. The MLRs models were developed in the R software V4.0.2 using the "caret" package models up to 5 variables were assessed to avoid overfitting (Cohen and Jensen 1997; Heinze and Dunkler 2017; Vittinghoff and McCulloch 2007). The evaluation of these MLRs was carried out using the R^2_{adj} and RMSE metrics. The variables producing models that comply with having a value of $R^2_{\text{adj}} \geq 0.5$ (Van Liew et al. 2003; Moriasi et al. 2007; Santhi et al. 2001) and an RMSE $\leq 15\%$ of the isotopic variability in the analyzed dataset (Moriasi et al. 2007; Singh et al. 2005) were considered as drivers of the isotopic composition of precipitation.

The procedure was applied to the complete isotopic dataset. In case no drivers of the isotopic composition of precipitation could be identified, the dataset was divided into seasons, i.e., DJF (December–February), MAM (March–May), JJA (June–August), and SON (September–November); and by the predominant air mass trajectories identified by the HYSPLIT model (section 3b). Despite having analyzed the isotopic composition of oxygen (δ^{18}O), hydrogen (δ^2H), and *d*-excess, only results for δ^{18}O and *d*-excess are presented because the results obtained with δ^{18}O and δ^2H were similar.

g. *Validation of findings in a regional context*

This aspect involved analysis of the isotopic composition of precipitation (δ^{18}O and *d*-excess) at the study site and stations from the Global Network of Isotopes in Precipitation (GNIP; IAEA/WMO 2021). Stations situated along different water vapor trajectories identified through the HYSPLIT model analysis and possessing at least one year of monthly collected isotopic data were used in the analysis. These included 10 stations located east (from the Brazilian coast) and 9 stations situated west (from the Galapagos Islands) of the Andean mountain range. A summary of the stations' metadata, geographical information, and isotopic data statistics as well as their source is presented in Tables S1 and S2 in the online supplemental material. The regional analysis consisted of determining the continental and isotopic effects of both the eastern and western slopes of the mountain range. These effects were assessed through linear regression between isotopic compositions and the elevation of the stations.

3. Results

a. *Description of meteorological conditions*

The intensity of precipitation corresponding to each of the samples collected for isotopic analysis rarely exceeded 10 mm day^{-1} (Fig. 3a). The events with the highest intensities occurred mainly in the period January–April, while events during the period July–October had the lowest intensities. The precipitation type and fraction corresponding to each of the collected rainfall samples showed that precipitation could usually be classified as light, followed by moderate and heavy precipitation (Fig. 3b). On a few occasions the presence of very heavy precipitation was observed. Average air temperature was lower during the less wet months (August–October) in comparison to the rest of the study period (Fig. 3c); average relative humidity was generally above 90% (Fig. 3d); average wind speed tended to be higher and solar radiation lower during the less wet months in comparison to the more humid periods (Figs. 3e and 3f, respectively). Table S3 in the supplemental material shows monthly values of the meteorological data used in this study for reference.

b. *Isotopic composition*

The δ^{18}O composition in precipitation at the study site varied between $-2.4‰$ and $-25.0‰$ with an arithmetic mean of $-11.9‰$ and a rainfall volume-weighted mean of $-10.5‰$, the δ^2H composition between $0.0‰$ and $-185.0‰$ with an

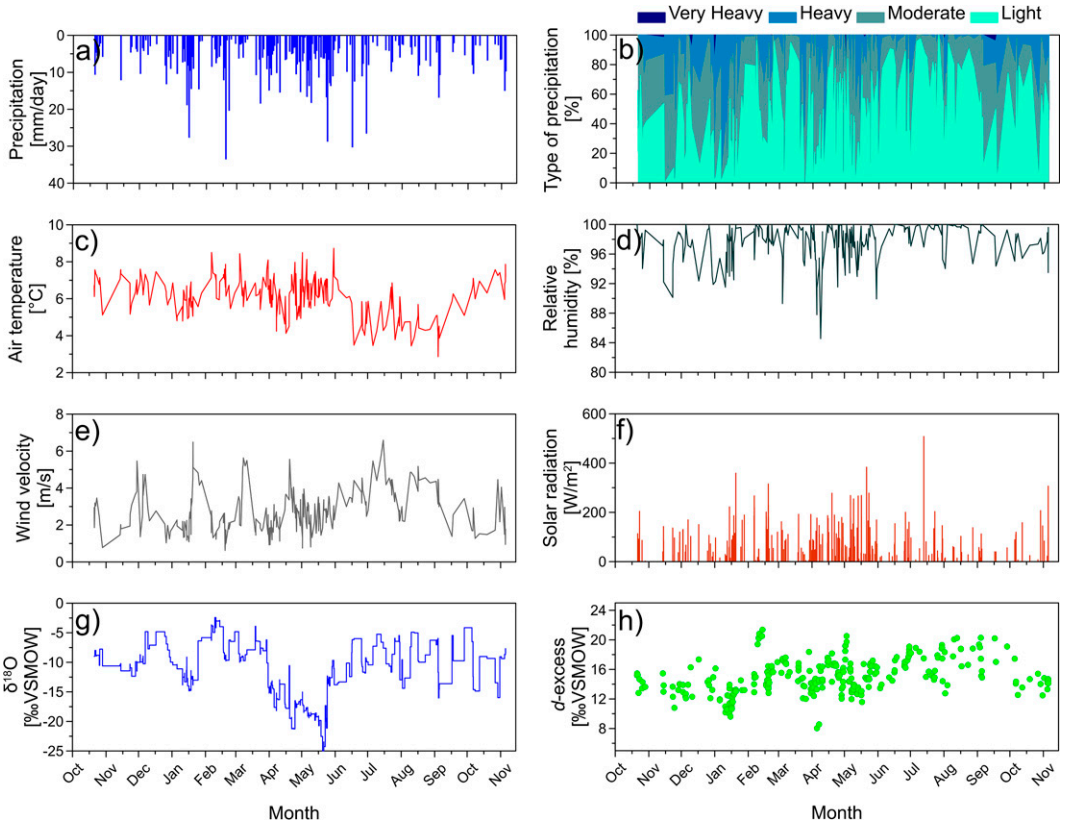

FIG. 3. Temporal variability of local (in situ) meteorological variables for each period a rainwater sample for isotopic analysis was collected and precipitation isotopic composition during the period November 2017–October 2018 at the Zhurucay Ecohydrological Observatory: (a) cumulative precipitation, (b) type and fraction of precipitation (from light to very heavy), (c) air temperature, (d) relative humidity, (e) wind velocity, (f) solar radiation, (g) $\delta^{18}O$, and (h) *d*-excess. The values in (c)–(f) represent the average value of local (in situ) meteorological variables during the period for which each water sample for isotope analysis was collected.

arithmetic mean of −80.4‰ and a rainfall volume-weighted mean of −68.5‰, and the *d*-excess between +8.0‰ and +21.4‰ with a mean of +15.0‰ (Figs. 3g,h). The $\delta^{18}O$ and $\delta^{2}H$ compositions decreased from March to May and the lowest values were observed in late May, while the highest isotope values observed during the rest of the study period. No clear seasonal variation was observed for *d*-excess. The slope of the LMWL (8.15) was similar to the one of the GMWL (8; Fig. 4). On the contrary, the intercept of the LMWL (+16.87‰) was larger than that of the GMWL (+10‰). Monthly statistics of the isotopic data used in this study are shown in the supplemental material (Table S3) for reference.

c. *Origin and trajectories of the vapor masses*

The 295 air mass back trajectories linked to local precipitation events are shown in Fig. 5. The transport of water vapor masses followed four main trajectories before reaching the study area. As revealed by the trajectory analysis, the Amazon basin (73.2%) represents the prevailing moisture source for the highlands in the southern region of Ecuador, which in turn resulted in relatively high *d*-excess values throughout the hydrological year. Other regions such as the Pacific coast basin (12.9%), Orinoco plains (11.2%), and Mato Grosso Massif (2.7%) contributed less to the regional moisture transport. Figure 5 also reveals that the air masses reaching the study site traveled through the different oceanic and continental regions considered as sources of atmospheric humidity. The air masses arriving from the Orinoco plains (Fig. 5a) originated in the tropical North Atlantic region (TNA), crossed the Orinoco basin (ORIC), continued through the northwestern part of the Northern Amazon region (NAMZ) crossing the southern part of Colombia and the northeastern region of Ecuador to reach the study area via the Andes [northern part of the Peru–Chile region (PECH)].

The air masses coming from the Pacific coast traveled over two main regions (Fig. 5b). The first group of air masses originated in the Caribbean Sea region (CABN), crossed the southern part of the Central America region (CAM) toward the Pacific Ocean, and then traveled through the western part of the tropical North Pacific region (TNP) until reaching the study area at the northern PECH region. The second group of air masses originated near the Pacific coast of southern Peru and reached the study area through the western part of the tropical South Pacific region (TSP). Atmospheric moisture arriving from the Mato Grosso Massif originated in two regions: 1) La Plata River basin (LPRB) and 2) Brazil's

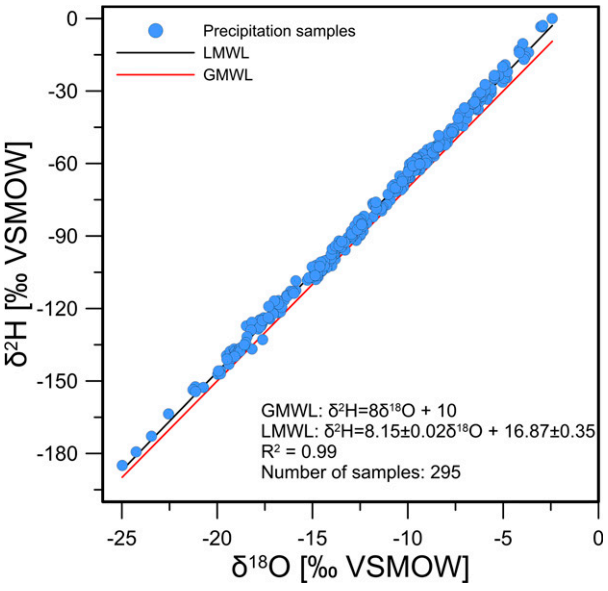

FIG. 4. δ^2H–δ^{18}O diagram constructed with the precipitation samples collected during the period November 2017–October 2018. The black linear fit indicates the local meteoric water line (LMWL) based on the samples presented in the study, and the red linear fit indicates the global meteoric water line (GMWL; Dansgaard 1964).

Northeast (NORD) regions (Fig. 5c). Independent from their origin, the air masses reached the study site traveling through the Tocantins basin (TOCA), Southern Amazon (SAMZ), and NAMZ regions.

Water vapor arriving from the Amazon basin and originated between latitudes 5°N–5°S crossed the equatorial Atlantic Ocean in the middle part of the TNA and tropical South Atlantic (TSA) regions (Fig. 5d). Once the air masses reached the Brazilian coast, they traveled through the northern part of the NORD and TOCA regions, the southern part of the Guyana region (GUYN), and the NAMZ region before reaching the study area.

The air masses coming from the Amazon basin and whose origin started south of 5°S originated in the middle part of the TSA region (Fig. 5e). After reaching the South American coast they mainly crossed the NORD, TOCA, and SAMZ regions until ascending to the study area through the southeastern part of the NAMZ region. The air masses from the Amazon basin at latitudes north of 5°N originated in the central part of the TNA region (Fig. 5f). Once these air masses reached the continent, they traveled through the GUYN and northern part of the NAMZ regions before converging in the study area.

d. Factors controlling the isotopic composition

Eighty predictive variables were obtained from the in situ meteorological data (local variables) and the HYSPLIT analysis (regional variables). The multicollinearity analysis (VIF) using a threshold value of 3 reduced the number of potential variables controlling the stable isotopic composition of precipitation for the complete study period, different seasons, and different trajectories. The number of remaining variables was 36 for the complete period, 26 for the DJF season, 34 for the MAM season, 23 for the JJA season, 21 for the SON season, 22 for the Orinoco plains, 20 for the Pacific Ocean, 11 for the Mato Grosso Massif, 27 for the Amazon basin with origin between latitudes 5°N and 5°S, 25 for the Amazon basin with origin at latitudes south of 5°S, and 27 for the Amazon basin with origin at latitudes north of 5°N. Those variables were used for the identification of the potential drivers of δ^{18}O and *d*-excess isotopic composition through correlation and linear regression analyses.

Results of the Spearman correlation analysis between δ^{18}O and *d*-excess and single local and regional meteorological variables showed low correlation values, i.e., lower than the $r < 0.7$ threshold. The explanation of the variance of those models was lower than 50% for both δ^{18}O and *d*-excess. Because of this, MLRs models considering datasets corresponding to the complete period, different seasons, and the main trajectories identified using HYSPLIT were built and evaluated. The results of the models that complied with the criteria used to define the drivers of the stable isotopic composition of precipitation, i.e., $R^2_{adj} \geq 0.5$ and RMSE $\leq 15\%$, are depicted in Table 1 and Fig. 6.

As shown in Table 1, it was possible to define key drivers of the δ^{18}O isotopic composition of precipitation using datasets for the whole study period and corresponding to the following trajectories: Orinoco plains, Pacific coast, and Mato Grosso Massif (Fig. 6). For the Amazon basin trajectories, the dataset was further split considering the origin of each trajectory since no MLR explaining more than 50% of the dataset variance was identified. Therefore, the Amazon basin dataset was divided into three origins considering their position with respect to the equator, namely, the trajectories with origin north of latitude 5°N, between latitudes 5°N and 5°S, and south of latitude 5°S. This spatial subclassification allowed identifying main drivers of the δ^{18}O isotopic composition of precipitation for samples arriving between latitudes 5°N and 5°S and latitudes below 5°S (Fig. 6). However, for the air masses arriving from the trajectories starting above latitude 5°N, no main drivers were identified using the complete period dataset. For this reason, we further split the dataset into seasons, and this permitted to identify governing features of the δ^{18}O isotopic composition of precipitation for the periods DJF, MAM, and SON (Table 1 and Fig. 6). We could not conduct the MLR evaluation for the period JJA due to the low number of observations to perform the analysis (Harrell 2015; Heinze and Dunkler 2017; Vittinghoff and McCulloch 2007).

Temp_i and Prec_5 explained 60.1% of the δ^{18}O composition of precipitation of the air masses arriving from the Orinoco Plains (Table 1). For the atmospheric moisture arriving from the Pacific coast, four variables, M+H+VH, Prec_1, RH_8, and RH_6, explained 58.1% of the δ^{18}O dataset variance, while for the Mato Grosso Massif air masses, RH_i, Prec_4, and SRad explained 93.8% of the δ^{18}O variance. Given the relatively low

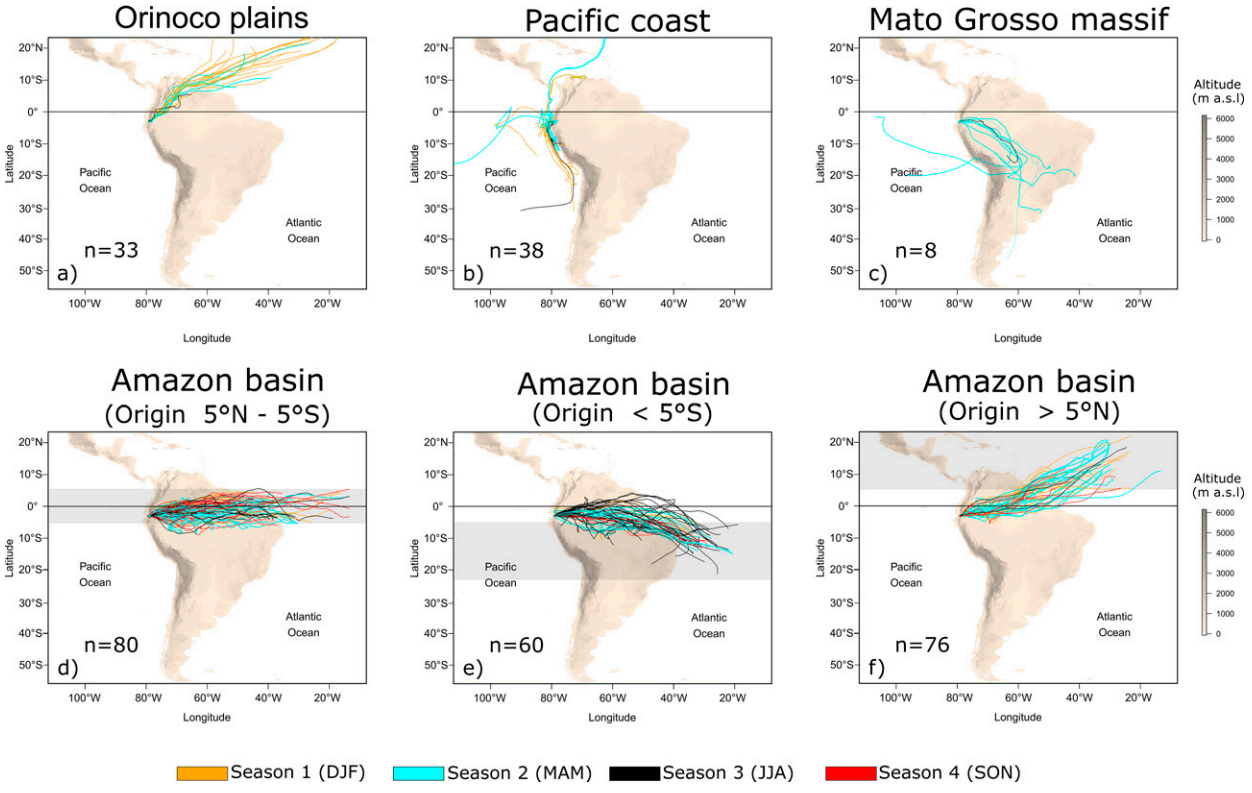

FIG. 5. Trajectories of the air masses reaching the study area during the period November 2017–October 2018 (n = 295) originating from (a) Orinoco plains, (b) Pacific coast, (c) Mato Grosso Massif, (d) Amazon basin with their origin between latitudes 5°N and 5°S, (e) Amazon basin with their origin below latitude 5°S, and (f) Amazon basin with their origin above latitude 5°N. The solid black line in the plots shows the 0° latitude for reference. Note: n = number of samples for each of the trajectories. The colors of the trajectories represent different sampling collection seasons: season 1 = December–February, season 2 = March–May, season 3 = June–August, and season 4 = September–November.

number of observations (n = 8) in comparison to the variables included in the MLR model for the latter, results need to be considered with care (Heinze and Dunkler 2017). Four variables, MD_4, $Prec_7$, $Prec_6$, and $Prec_3$, explained 56.2% of the $\delta^{18}O$ composition variance for the Amazon air masses originating between latitudes 5°N and 5°S. For the atmospheric moisture traveling through the Amazon basin and coming from latitudes south of 5°S four variables, $Temp_i$,

TABLE 1. Summary statistics of the multiple linear regression models (MLRs) for $\delta^{18}O$ complying with the criteria to define controllers of the stable isotopic composition of precipitation using the stepwise criterion. An asterisk indicates that samples collected during the complete study period were included in the MLRs. For the Amazon basin > 5°N trajectories, S1, S2, and S4 indicate the dataset was further split into different seasons as follows: S1 = December–February, S2 = March–May, and S4 = September–November. In situ variables: $Temp_i$ = in situ air temperature, $Press_i$ = in situ atmospheric pressure, HR_i = in situ relative humidity, SRad = in situ solar radiation, H + VH (accumulated fraction of heavy and very heavy precipitation), M + H + VH (accumulated fraction of moderate, heavy, and very heavy precipitation). Regional variables: MD_x = mix depth, $SRad_x$ = regional solar radiation, $Prec_x$ = regional precipitation), RH_x = regional relative humidity. The subscript numbers next to the regional variables indicate the number of days backward according to the trajectories identified by the HYSPLIT model; n = number of samples used for the MLRs, m = number of variables used to obtain the MLRs, R^2 = R squared, R^2_{adj} = adjusted R squared, AIC = Akaike information criteria, and RMSE = root-mean-square error.

Trajectories	Variables	n	m	R^2	R^2_{adj}	AIC	RMSE	p value
Orinoco plains*	$Temp_i$, $Prec_5$	33	2	0.60	0.57	161.06	2.46	1.05×10^{-6}
Pacific coast*	M + H + VH, $Prec_1$, RH_8, RH_6	38	4	0.58	0.53	191.51	2.57	6.27×10^{-6}
Mato Grosso Massif*	RH_i, $Prec_4$, $SRad_i$	8	3	0.94	0.89	32.54	0.99	7.08×10^{-3}
Amazon basin (5°N–5°S)*	MD_4, $Prec_7$, $Prec_6$, $Prec_3$	80	4	0.56	0.53	425.57	3.21	8.09×10^{-13}
Amazon basin < 5°S*	$Temp_i$, $Press_i$, RH_6, H + VH	60	4	0.53	0.50	327.39	2.72	2.15×10^{-8}
Amazon basin > 5°N—S1	$SRad_1$, $Temp_i$, $SRad_2$	26	3	0.58	0.53	123.07	2.13	1.97×10^{-4}
Amazon basin > 5°N—S2	$Press_i$, RH_3,	39	2	0.54	0.52	229.81	3.28	4.53×10^{-4}
Amazon basin > 5°N—S4	RH_2	9	1	0.67	0.62	36.22	1.29	7.29×10^{-3}

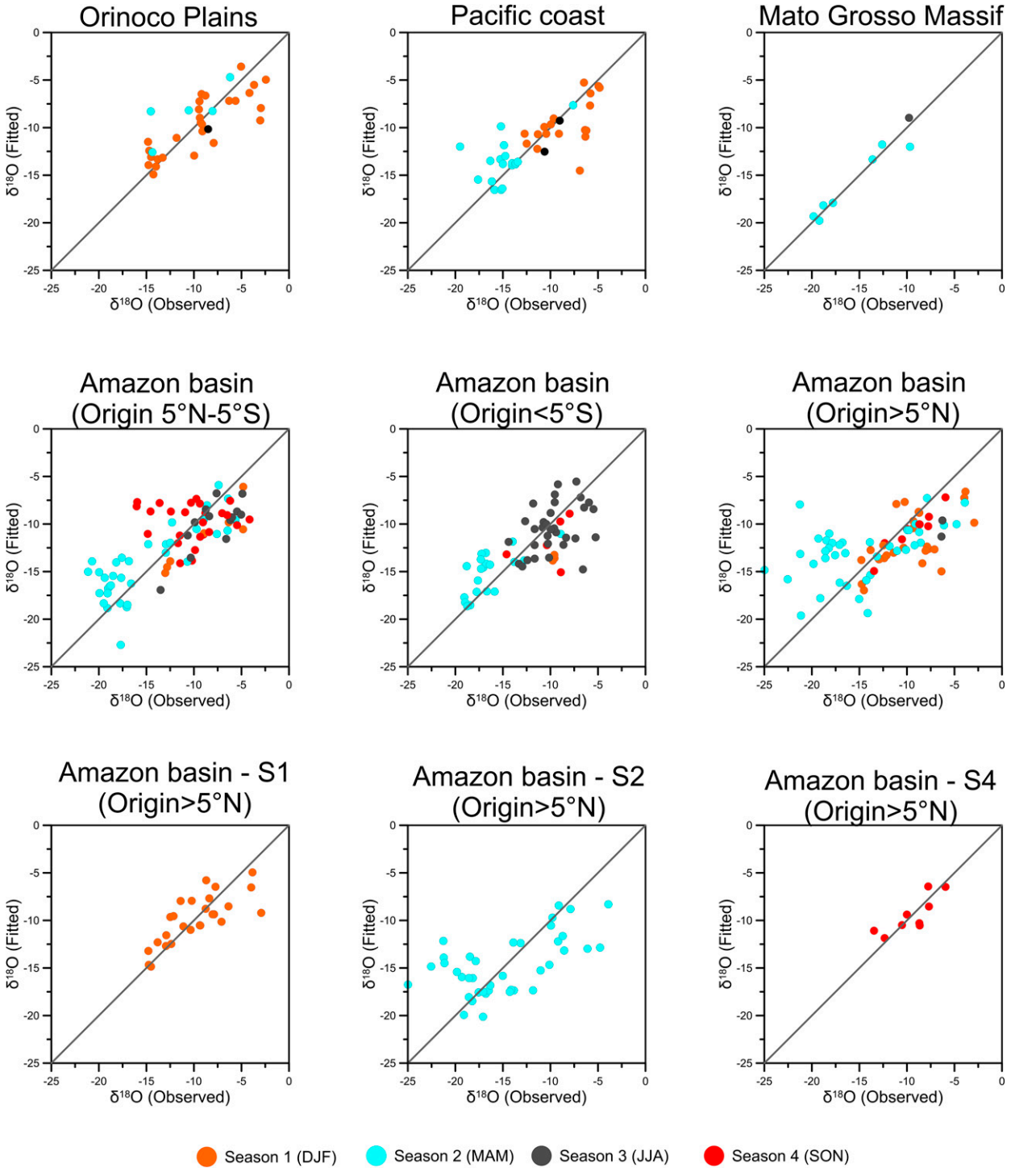

FIG. 6. Scatterplots of the observed and modeled $\delta^{18}O$ isotopic composition using multiple linear regression models (MLRs) complying with the criteria to define key drivers of the stable isotopic composition of precipitation according to the air mass back trajectories identified using HYSPLIT. An asterisk indicates that samples collected during the complete study period were included in the MLRs. For the Amazon basin > 5°N trajectories, the colors of the circles represent different sampling collection seasons: season 1 (S1) = December–February, season 2 (S2) = March–May, season 3 (S3) = June–August, and season 4 (S4) = September–November.

$Press_i$, RH_6, and H+VH, explained 53.4% of the variance of the $\delta^{18}O$ composition of precipitation.

Regarding the Amazon air masses originating at latitudes above 5°N, three variables, $SRad_1$, $Temp_i$, and $SRad_2$, explained 58.4% of the $\delta^{18}O$ isotopic signal variance during the period DJF. $Press_i$ and RH_3 explained more than half of the variance (54.4%) of the $\delta^{18}O$ isotopic signal of precipitation during the period MAM. For the period SON, a single variable (RH_2) explained more than half of the $\delta^{18}O$ isotopic signal variance (66.6%). For *d*-excess, we did not find MLRs explaining at least 50% of the variance either by splitting the complete dataset of the isotopic signal by season or by considering the trajectories of the air masses forming local precipitation.

4. Discussion

a. Isotopic composition

The isotopic composition of precipitation showed lower $\delta^{18}O$ and $\delta^{2}H$ values during the wettest periods (April–May) and higher values during the less wet ones (August–September) (Fig. 3). Similar findings were reported by Esquivel-Hernández et al. (2019) and Mosquera et al. (2016a) for the Andean Páramo of southern Ecuador. Depleted values are likely related to the passage of the ITCZ over the Ecuadorian Andes and the Amazon basin and are associated with the convective activity of the region (Gastmans et al. 2017; Rozanski and Araguas 1995). Enriched values are likely the result from the recycling of moisture stemming from the Ecuadorian Amazon. This moisture is not influenced by local re-evaporation of the subcloud due to the short distance between the base of the cloud and the Andes and by the low moisture saturation deficit (Muñoz et al. 2016).

The similarity between the slopes of the LMWL and GMWL (Fig. 4) indicates that fractionation by evaporation of raindrops does not occur locally, i.e., at the study area (e.g., in the subcloud), as has been observed in other regions (Dinçer and Payne 1971). Since most ~87% of the total vapor masses arrive from the east side of the Andean cordillera regardless of their trajectory (Fig. 5), the higher intercept of the LMWL compared to the GMWL mainly relates to the passage of the air masses through the Ecuadorian Amazon, with a large continental effect (i.e., at regional scale). That is, water vapor high in *d*-excess, which has undergone isotopic fractionation under nonequilibrium conditions due to evaporation and transpiration as it passes across the Amazon rain forest, accumulates, and subsequently rises by orographic effects to the study site. Gastmans et al. (2017) also reported larger intercept values of the LMWL, between +12‰ and 13‰, at stations located along the Amazon rain forest. They attributed those observations to water vapor recirculation. To a lesser extent, this effect could also be the result of the transport of moisture from the west undergoing isotopic fractionation under nonequilibrium conditions as it travels from the coast to the colder Andes as previously suggested by Mosquera et al. (2016a).

b. Origin and trajectories of vapor masses

The dominance of air masses arriving from the eastern side of the Andes (87.1%; Fig. 5) agrees with other studies reporting that moisture from the Atlantic Ocean traveling through the Amazon rainforest is the main source of humidity to the region (Arias et al. 2015; Espinoza et al. 2020). The lower contribution from the Pacific Ocean to local precipitation (12.9%) is in line with prior findings of Esquivel-Hernández et al. (2019). The trajectories of water vapor masses identified in our study coincide with those reported in previous studies in the Ecuadorian Andes (Esquivel-Hernández et al. 2019; Windhorst et al. 2013). This fact provides confidence that the Lagrangian models are adequate to track humidity pathways across the Andean region.

Regardless of their origin and atmospheric pathways, air masses forming local precipitation are affected by different low-level jets, which transport large amounts of moisture in South America. Among these, the Orinoco low-level jet (OLLJ; Jiménez-Sánchez et al. 2020) influences the air masses crossing the Orinoco plains. Air masses stemming from the Pacific coast are influenced by the Chocó low-level jet (Chocó-LLJ) (Arias et al. 2015; Sakamoto 2011) being the product of atmosphere–ocean–land interactions, which rises by orographic effect from the tropical Andes to interact with the warmer trade winds from the east of the mountain range. Air masses coming from both the Guiana Massif and the Amazon rainforest are affected by the South American low-level jet (SALLJ) in which water vapor entering the Amazon River basin mixes with recycled moisture. This effect, in turn, increases the moisture for precipitation at nearby regions (Montini et al. 2019; Poveda et al. 2014).

c. Factors controlling the isotopic composition of precipitation

The geographical context of the Andes has important implications in local and regional meteorology across South America. Accordingly, a combination of local and regional meteorological variables generally explained the temporal variability of the stable isotopic composition in the highlands of southern Ecuador regardless of the trajectory of atmospheric moisture forming local rainfall (Table 1). It is worth noting that although multicollinearity and correlation analyses precluded the inclusion of redundant information in the MLRs, they also restrict the possibility of directly comparing explanatory variables among the models identified for each of the trajectories. Nevertheless, these variables allow obtaining improved understanding of rainfall formation processes as described below.

Because of its influence on isotopic fractionation, local temperature is a factor often found to influence precipitation's isotopic composition in tropical and nontropical latitudes (e.g., Dansgaard 1964; Kattan 2019; Le Duy et al. 2018). Accordingly, $Temp_i$ influences the $\delta^{18}O$ isotopic composition of precipitations arriving from the Orinoco plains. The HYSPLIT analysis revealed that it takes about 5 days for the air masses transported via OLLJ to reach the study site, justifying the presence of the regional variable

$Prec_5$ as an important predictor of the $\delta^{18}O$ composition. Both variables revealed the prevalence of a strong rain-out process over this basin before reaching the Ecuadorian highlands. The activity of the OLLJ is higher during the DJF season (Jiménez-Sánchez et al. 2020), explaining why the majority of precipitation samples from the Orinoco plains were collected during this season (Fig. 6).

Air masses originating from the Pacific coast are affected by the Chocó LLJ and produce very intense rain showers in the study area (Poveda et al. 2014). This effect explains the presence of precipitation occurring nearby ($Prec_1$) and the most intense fraction of local precipitation (M + H + VH) in the MLR of this trajectory (Table 1). These findings are in line with the study of Hagemans et al. (2021), who reported that for a study site near the ZEO in the period 2013–17, the most intense rainfall events arrived from the west flank of the Andean Cordillera. Convective activity at our study site is favored by a higher thermal breeze and moist air advection (Orellana-Alvear et al. 2017), leading to lower isotopic values (Hu et al. 2018; Kurita 2013) and reaffirming the presence of these variables in the MLR model. Moisture transport by the Chocó-LLJ can be traced as far as 30°S, down to the coast of Chile (Poveda et al. 2014; Sakamoto 2011). Humidity carried by those air masses likely influences precipitation formation at the study site, as indicated by the regional variables (RH_8 and RH_6) included in the model. The Chocó-LLJ is weaker in DJF when it preferentially moves to regions near the equator (Poveda et al. 2014), bringing in this period higher amounts of rainfall to Ecuador (Poveda et al. 2014), and explaining that most samples of the Pacific trajectory were collected during this season (Fig. 6).

As a result of their influence on isotopic fractionation processes, local environmental variables have been reported to influence the isotopic composition of precipitation (Kattan 2019; Le Duy et al. 2018). At our study area, isotopic fractionation of air masses arriving from the Mato Grosso Massif is locally controlled by air humidity (RH_i) and the amount of incoming solar energy ($SRad_i$). Since the area where the air masses following this trajectory (travel time 4 days) coincides with the SAMZ region, the variable $Prec_4$ highlights the influence of the south Amazon rain forest in the precipitation formation at the south Ecuadorian highlands, particularly during the wettest MAM season (Fig. 6). Concomitant with the evolution of the Amazonian mesoscale convective systems to a dominant monsoon flux (Aceituno 1988; Arvor et al. 2014; Zhou and Lau 1998), the samples corresponding to this trajectory were collected during the MAM season, which likely explains their isotopically depleted values.

Air masses arriving from the Amazon basin, between latitudes 5°N–5°S, were the only ones whose isotopic composition was solely controlled by regional climatological variables (Table 1). This finding suggests that humidity originated from the Atlantic Ocean ($Prec_6$ and $Prec_7$) is transported to the continent by trade winds. It subsequently crosses the Amazon rain forest where turbulent convection favors the mixture of the air masses (MD_4) with local humidity generated by the transpiration activity of the Amazon rain forest ($Prec_3$), reaching its peaks in the period May–November (Doughty and Goulden 2008). Foregoing explains why most of the precipitation samples stemming from this trajectory were collected during this period (Fig. 6). It also explains the importance of moisture transport from the tropical Atlantic region through the Amazon basin in rainfall formation processes in the Ecuadorian Andes.

Changes in atmospheric pressure ($Press_i$) are likely to produce an adiabatic lapse rate (Ingraham. 1998; Rindsberger et al. 1983). Such changes in turn exert direct control over temperature ($Temp_i$) and indirectly over the isotopic composition of precipitation (Kattan 2019; Le Duy et al. 2018). This process in addition to convective activity occurring at the study site (H + VH) (Orellana-Alvear et al. 2017) locally influence the isotopic composition of air masses arriving from the Amazon basin south of the 5°S latitude. These findings further support previous studies reporting that convective processes can control the isotopic composition of precipitation at tropical latitudes (Kurita 2013; Nlend et al. 2020; Sánchez-Murillo et al. 2016). Regionally, the SALLJ—responsible for bringing humidity to several regions across South America (Angelis and Salio 2006)—plays an important role in convective systems (Wang and Paegle 1996) and transports moisture to the Andes (Jones 2019). This effect explains the presence of the RH_6 variable in the MLR model of this trajectory, suggesting that the eastern coastline of South America is the region via which atmospheric humidity enters the continent. Moreover, strong winds across the southern part of the Amazon Forest transport large amounts of moisture to the Andean highlands during the JJA season (Montini et al. 2019), explaining why most of the samples corresponding to this air mass trajectory were collected during this period (Fig. 6).

The $\delta^{18}O$ composition of precipitation from the Amazon basin originating above the 5°N latitude is influenced by several factors depending on the season. Nevertheless, these factors correspond to in situ or nearby regional atmospheric conditions occurring up to 3 days before local precipitation is triggered regardless of the period of analysis (Table 1). In general, atmospheric humidity from the Atlantic Ocean is carried to the continent by trade winds (Fig. 5f). Passing the Amazon, these air masses gain large amounts of moisture due to transpiration of the rain forest as indicated by the presence of the variables RH_3, RH_2, $Srad_1$, and $Srad_2$ in the MLR models (Angelis and Salio 2006; Vera and Douglas 2006). Considering the depleted isotopic values along this trajectory, these findings further emphasize the influence of convective processes on precipitation formation and are a sign of mesoscale convective systems generated over the rain forest a few days before atmospheric moisture reaches the study area. After that, the air masses continue along the eastern edge of the Andes and reach the study site where in situ meteorological conditions ($Press_i$ and $Temp_i$) influence the $\delta^{18}O$ isotopic composition of local precipitation (Kattan 2019; Le Duy et al. 2018).

While our MLRs analysis was able to explain between 53% and 94% of the $\delta^{18}O$ dataset variance (Table 1), we recognize that discrepancies between observed and modeled values remain (Fig. 6). Based on the air mass trajectories identified in

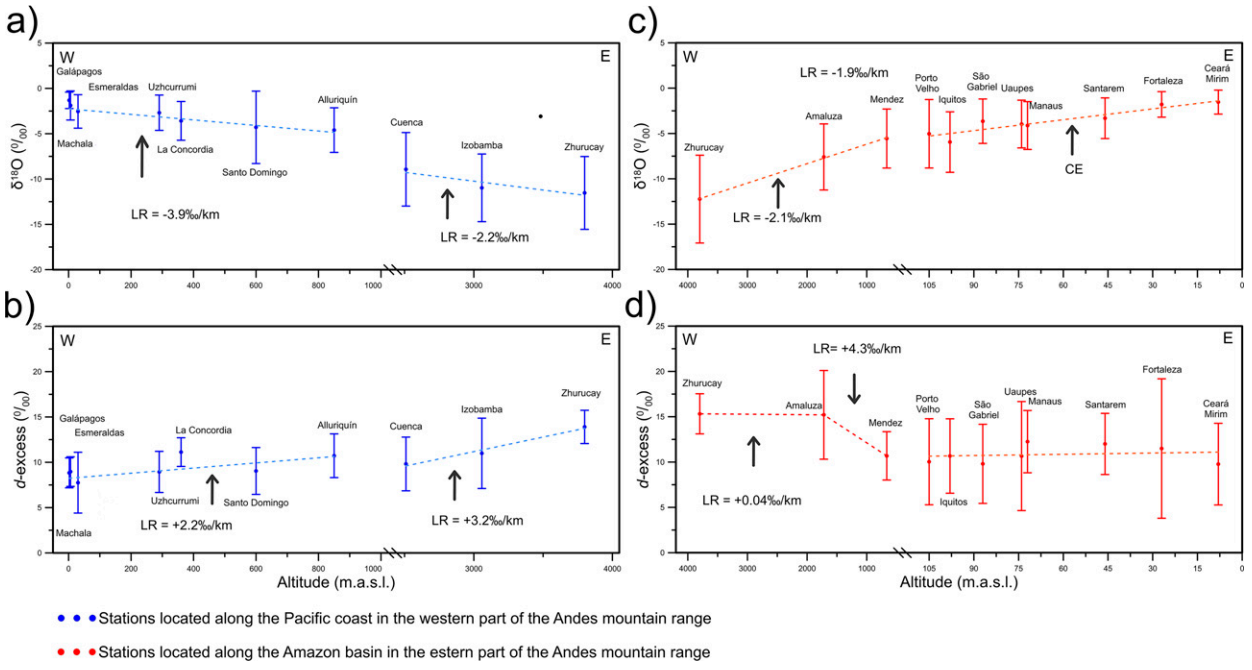

FIG. 7. δ^{18}O and *d*-excess continental effect (CE) and altitudinal lapse rate (LR) from different moisture sources for both the (a),(b) western and (c),(d) eastern slopes of the Andean mountain range. The δ^{18}O and *d*-excess error bars represent $\pm 1\sigma$. Note the break of the *x* axis in the subplots. Data outside the study area were retrieved from the Global Network of Isotopes in Precipitation (GNIP) database (IAEA/WMO 2021). Metadata, geographical information, isotopic data statistics, and source of the GNIP stations used in this analysis are presented in Tables S1 and S2 in the supplemental material.

our study, these discrepancies likely result from the interaction of continental versus maritime effects influencing precipitation formation processes in the tropical Andes (Vuille et al. 2000). This finding suggests the need for 1) longer isotope time series, 2) high-frequency sampling across Pacific and Atlantic altitudinal transects, 3) water vapor sampling, and/or 4) other types of atmospheric information (e.g., radar and/or vertical water column characteristics or sounding profiles) to further improve process-based understanding of rainfall formation in the region.

Key drivers for *d*-excess in precipitation could not be identified. This is likely because most of the air masses stemming from the east side of the Andean cordillera crossed the Ecuadorian Amazon (NAMZ and SAMZ regions; Fig. 5), where water vapor high in *d*-excess—as a result of forest re-evaporation and transpiration processes—accumulates and is lifted by orography to the Andean highlands. This process likely explains the low temporal variability of *d*-excess at the study site which precludes finding factors influencing *d*-excess in local precipitation.

d. Validation of findings in a regional context

The δ^{18}O composition of precipitation decreases as a result of strong continental (CE) and altitudinal or lapse rate (LR) effects on the east side of the Andean mountain range (Fig. 7a). The CE is observed from the Atlantic coast of Brazil (Ceará Mirin with a value of $-1.53‰$ at 8 m MSL) to almost the middle part of the Amazon basin (Porto Velho with a value of $-5.03‰$ at 105 m MSL). A clear δ^{18}O isotopic LR of $-2.1‰$ km^{-1} was observed from the Ecuadorian Amazon (Mendez with a value of $-5.56‰$ at 665 m MSL) to the study area (Zhurucay with a value of $-11.85‰$ at 3800 m MSL), which agrees with tropical and subtropical lapse rates (Sánchez-Murillo et al. 2020). The identified LR reaffirms the drivers of the δ^{18}O isotopic composition obtained for the trajectories coming from the Amazon basin, which are strongly influenced by the transport of air masses from the Atlantic Ocean across the entire Amazon basin via the SLLJ before ascending the Andes toward the study site.

Regarding the spatial variation of *d*-excess east of the Andes (Fig. 7b), the composition remains very uniform from the coast of Brazil (Ceará Mirim with $+9.77‰$ at 8 m MSL) to Porto Velho ($+10.03‰$ at 105 m MSL). In contrast, *d*-excess values increased significantly from Mendez ($+10.68‰$ at 665 m MSL, at the lowland of the Ecuadorian Amazon) to Amaluza ($+15.20‰$ at 1720 m MSL, near the Andes–Amazon transition in south Ecuador), with an overall LR of $+4.3‰$ km^{-1}. This rate is much higher than the $+1‰$ km^{-1} pantropical LR of *d*-excess reported by Sánchez-Murillo et al. (2020) and is close to the upper limit of the range of *d*-excess LR values previously reported for high-elevation regions worldwide, which vary between $+1.3‰$ and $+4.0‰$ km^{-1} (Bershaw et al. 2012; Esquivel-Hernández et al. 2019; Gonfiantini et al. 2001). Further on, from Amaluza to the study area ($+15.32‰$ at 3800 m MSL), *d*-excess remained almost constant ($+0.04‰$ km^{-1}), indicating that the isotopic composition of water vapor arriving from the east to the study site was unaffected by fractionation processes as it orographically

ascended the Andean hillslopes toward Zhurucay. The latter supports the inference that large amounts of recycled moisture from the transpiration activity of the Amazon Forest (Doughty and Goulden 2008) contribute to precipitation formation at the south Ecuadorian highlands for almost all trajectories arriving east of the Andes, regardless of their specific origin as evidenced by the very small variation of *d*-excess in local precipitation.

West of the Andes, a strong $\delta^{18}O$ isotopic LR is observed (Fig. 7c). From the maritime domain of Galapagos (−1.31‰ at 2 m MSL) to the Pacific slope of Ecuador at Alluriquín (−4.6‰ at 850 m MSL), an LR of −3.9‰ km^{-1} was identified. At higher elevations, from Cuenca (−8.93‰ at 2510 m MSL) to the study site (−11.85‰ at 3800 m MSL) a $\delta^{18}O$ isotopic LR of −2.2‰ km^{-1} was found, which is within the range of values identified across the tropics (from −1.5‰ to −2.7‰ km^{-1}; Sánchez-Murillo et al. 2020). This LR is slightly higher than the one reported by Gébelin et al. (2021) in the west-facing slopes of the Western Cordillera in south Ecuador based on the $\delta^{18}O$ isotopic composition of stream waters (−1.5‰ km^{-1}). Overall, the LR analysis within the Pacific slope supports well both the in situ (M + H + VH, $Prec_1$) and regional variables (HR_8, and HR_6) influencing the $\delta^{18}O$ composition of precipitation, as the Chocó-LLJ transport mechanism is associated with mesoscale convective systems resulting in heavy rains (Poveda et al. 2014), explaining the identified depleted isotopic values.

For *d*-excess in the western slope (Fig. 7d), the maritime domain from Galapagos (+8.83‰ at 2 m MSL) to the Pacific slope at Alluriquín (+10.72‰ at 850 m MSL), there is a relatively small isotopic variation (+2.2‰ km^{-1}). This may be related to large humidity contributions from the Pacific Ocean. Above 2500 m MSL, *d*-excess values increase at a higher rate (+3.2‰ km^{-1}) from Cuenca (+9.82‰ at 2510 m MSL) to the study site (+13.91‰ at 3800 m MSL). This may be because in the colder regions of the Ecuadorian Andes air masses undergo fractionation under nonequilibrium conditions due to complex orographic effects, (Esquivel-Hernández et al. 2019).

5. Conclusions

The study reports the isotopic composition of precipitation during rainstorm events in a tropical alpine Páramo area (3800 m MSL) in southern Ecuador, and the trajectories followed by the air masses that transport water vapor to the experimental site during the period November 2017–October 2018. Four predominant moisture sources were identified, namely, the Amazon basin (73.2%), the Pacific Ocean (12.9%), the Orinoco plains (11.2%), and the Mato Grosso Massif (2.7%). For the different trajectories, a combination of local and regional factors was identified to drive the $\delta^{18}O$ isotopic composition of precipitation. These factors included temperature, pressure, relative humidity, and a fraction of different precipitation types, particularly related to heavy rainfall, indicating that convective processes influence the stable isotopic composition of precipitation. On the contrary, the low temporal variability of *d*-excess did not permit to explain the variance of the available dataset, and thus no drivers of this isotopic parameter could be identified. Nonetheless, the identified high *d*-excess values during the study period highlight the important contribution of moisture recycled from the Amazon Forest. Our study offers a most needed baseline to underpin key drivers controlling precipitation formation across the Andean highlands with strong implications for isotope-based paleoclimate reconstructions and testing and validation of climate models in the region.

Acknowledgments. The manuscript is an outcome of the Master of Science Program in Hydrology of the University of Cuenca (UC). Thanks are due to INV Metals S.A. for logistic assistance in the fieldwork at the Zhurucay Experimental Observatory. We acknowledge the support of Comuna Chumblín Sombrederas (San Fernando, Azuay) for offering access to the community land reserve. Thanks are due to Irene Cardenas for carrying out the laboratory analyses, the researchers and students of the Department of Water Resources and Environmental Sciences (iDRHICA) of UC for supporting field monitoring, Prof. Jan Feyen for editorial assistance, and Polona Vreča and one anonymous reviewer for their constructive criticism that helped improving the quality of the manuscript. We acknowledge the contribution of the Vice-rectorate for Research of the University of Cuenca (VIUC) through the project "High-Resolution Radar Analysis of Precipitation Extremes in Ecuador and North Peru and Implications of the ENSO-Dynamics." Author contributions: Conceptualization and methodology: G.M.M., G.E.H., and P.C. Data curation and analysis: D.Z. Literature review: D.Z. and G.M.M. Writing—original draft: D.Z. and G.M.M. Writing—review and editing: G.M.M., G.E.H., M.C., R.S.M, J.O.A., and P.C. Funding acquisition: G.M.M. Project administration: G.M.M. Supervision: G.M.M. All authors have read and agreed to the published version of the manuscript. The authors declare no conflict of interest. Funding: This research was funded by the IAEA research contract 22905 and the Central Research Office of the UC (DIUC) in the framework of the project "Identification of Tap Water Sources and Water Supply Structure in a Mesoscale Tropical Andean City." G.M.M. is supported by a Postdoctoral Fellowship from Universidad San Francisco de Quito and the H2020 European Research and Innovation action Grant Agreement 869226 (DRYvER). Participation of J.O-A was funded by Deutsche Forschungsgemeinschaft under Grant RO 3815/2-1.

Data availability statement. The data supporting the findings of this study are available from the corresponding author upon reasonable request.

REFERENCES

Aceituno, P., 1988: On the functioning of the Southern Oscillation in the South American Sector. Part I: Surface climate. *Mon. Wea. Rev.*, **116**, 505–524, https://doi.org/10.1175/1520-0493(1988)116<0505:OTFOTS>2.0.CO;2.

Agudelo, J., P. A. Arias, S. C. Vieira, and J. A., Martínez, 2018: Influence of longer dry seasons in the Southern Amazon on patterns of water vapor transport over northern South America and the Caribbean. *Climate Dyn.*, **52**, 2647–2665, https://doi.org/10.1007/s00382-018-4285-1.

Angelis, C. F., and P. Salio, 2006: Impacts of the low level jets on the precipitation over Southern South America. *Proc. of 8 ICSHMO*, Foz do Iguaçu, Brazil, INPE, 961–966, http://mtc-m16b.sid.inpe.br/col/cptec.inpe.br/adm_conf/2005/11.01.00.06/doc/961-966.pdf.

Araguás-Araguás, L., K. Froehlich, and K. Rozanski, 2000: Deuterium and oxygen-18 isotope composition of precipitation and atmospheric moisture. *Hydrol. Processes*, **14**, 1341–1355, https://doi.org/10.1002/1099-1085(20000615)14:8<1341::AID-HYP983>3.0.CO;2-Z.

Arias, P. A., J. A. Martínez, and S. C. Vieira, 2015: Moisture sources to the 2010–2012 anomalous wet season in northern South America. *Climate Dyn.*, **45**, 2861–2884, https://doi.org/10.1007/s00382-015-2511-7.

Arvor, D., V. Dubreuil, J. Ronchail, M. Simões, and B. M. Funatsu, 2014: Spatial patterns of rainfall regimes related to levels of double cropping agriculture systems in Mato Grosso (Brazil). *Int. J. Climatol.*, **34**, 2622–2633, https://doi.org/10.1002/joc.3863.

Bershaw, J., S. M. Penny, and C. N. Garzione, 2012: Stable isotopes of modern water across the Himalaya and eastern Tibetan Plateau: Implications for estimates of paleoelevation and paleoclimate. *J. Geophys. Res.*, **117**, D02110, https://doi.org/10.1029/2011JD016132.

Ciric, D., M. Stojanovic, A. Drumond, R. Nieto, and L. Gimeno, 2016: Tracking the origin of moisture over the Danube River Basin using a Lagrangian approach. *Atmosphere*, **7**, 162, https://doi.org/10.3390/atmos7120162.

Cohen, P. R., and D. Jensen, 1997: Overfitting explained. *Preliminary Papers of the Sixth Int. Workshop on Artificial Intelligence and Statistics*, Fort Lauderdale, FL, PMLR, 115M–122, http://proceedings.mlr.press/r1/cohen97a/cohen97a.pdf.

Córdova, M., G. Carrillo-Rojas, P. Crespo, B. Wilcox, and R. Célleri, 2015: Evaluation of the Penman-Monteith (FAO 56 PM) method for calculating reference evapotranspiration using limited data. *Mt. Res. Dev.*, **35**, 230–239, https://doi.org/10.1659/MRD-JOURNAL-D-14-0024.1.

Craig, H., 1961: Isotopic variations in meteoric waters. *Science*, **133**, 1702–1703, https://doi.org/10.1126/science.133.3465.1702.

Dansgaard, W., 1964: Stable isotopes in precipitation. *Tellus*, **16**, 436–468, https://doi.org/10.3402/tellusa.v16i4.8993.

Dinçer, T., and B. R. Payne, 1971: An environmental isotope study of the south-western Karst region of Turkey. *J. Hydrol.*, **14**, 233–258, https://doi.org/10.1016/0022-1694(71)90037-0.

Doughty, C. E., and M. L. Goulden, 2008: Seasonal patterns of tropical forest leaf area index and CO_2 exchange. *J. Geophys. Res.*, **113**, G00B06, https://doi.org/10.1029/2007JG000590.

Draxler, R. R., and G. D. Hess, 1998: An overview of the HYSPLIT_4 modeling system of trajectories, dispersion, and deposition. *Aust. Meteor. Mag.*, **47**, 295–308.

Espinoza, J. C., and Coauthors, 2020: Hydroclimate of the Andes part I: Main climatic features. *Front. Earth Sci.*, **8**, 1–20, https://doi.org/10.3389/feart.2020.00064.

Esquivel-Hernández, G., and Coauthors, 2019: Moisture transport and seasonal variations in the stable isotopic composition of rainfall in Central American and Andean Páramo during El Niño conditions (2015–2016). *Hydrol. Processes*, **33**, 1802–1817, https://doi.org/10.1002/hyp.13438.

Froehlich, K., M. Kralik, W. Papesch, D. Rank, H. Scheifinger, and W. Stichler, 2008: Deuterium excess in precipitation of Alpine regions – Moisture recycling. *Isotopes Environ. Health Stud.*, **44**, 61–70, https://doi.org/10.1080/10256010801887208.

Gastmans, D., and Coauthors, 2017: Controls over spatial and seasonal variations on isotopic composition of the precipitation along the central and eastern portion of Brazil. *Isotopes Environ. Health Stud.*, **53**, 518–538, https://doi.org/10.1080/10256016.2017.1305376.

Gébelin, A., C. Witt, M. Radkiewicz, and A. Mulch, 2021: Impact of the Southern Ecuadorian Andes on oxygen and hydrogen isotopes in precipitation. *Front. Earth Sci.*, **9**, 1–9, https://doi.org/10.3389/feart.2021.664590.

Gimeno, L., 2013: Grand challenges in atmospheric science. *Front. Earth Sci.*, **1**, 1–5, https://doi.org/10.3389/feart.2013.00001.

Gonfiantini, R., M. A. Roche, J. C. Olivry, J. C. Fontes, and G. M. Zuppi, 2001: The altitude effect on the isotopic composition of tropical rains. *Chem. Geol.*, **181**, 147–167, https://doi.org/10.1016/S0009-2541(01)00279-0.

Hagemans, K., and Coauthors, 2021: Patterns of alluvial deposition in Andean lake consistent with ENSO trigger. *Quat. Sci. Rev.*, **259**, 106900, https://doi.org/10.1016/j.quascirev.2021.106900.

Hair, J. F., Jr., G. T. M. Hult, C. Ringle, and M. Sarstedt, 2016: *A Primer on Partial Least Squares Structural Equation*. Sage Publications, 384 pp.

Harrell, F. E., 2015: *Regression Modeling Strategies*. 2nd ed. Springer, https://doi.org/10.1007/978-3-319-19425-7.

He, S., N. F. Goodkin, D. Jackisch, M. R. Ong, and D. Samanta, 2018: Continuous real-time analysis of the isotopic composition of precipitation during tropical rain events: Insights into tropical convection. *Hydrol. Processes*, **32**, 1531–1545, https://doi.org/10.1002/hyp.11520.

Heinze, G., and D. Dunkler, 2017: Five myths about variable selection. *Transplant Int.*, **30**, 6–10, https://doi.org/10.1111/tri.12895.

Helsel, D. R., and R. M. Hirsch, 2002: Statistical methods in water resources. Techniques of Water-Resources Investigations 04-A3, USGS, 510 pp., https://doi.org/10.3133/twri04A3.

Heydarizad, M., E. Raeisi, R. Sori, and L. Gimeno, 2019: An overview of the atmospheric moisture transport effect on stable isotopes (^{18}O, ^{2}H) and *d*-excess contents of precipitation in Iran. *Theor. Appl. Climatol.*, **138**, 47–63, https://doi.org/10.1007/s00704-019-02798-9.

Hu, J., J. Emile-Geay, J. Nusbaumer, and D. Noone, 2018: Impact of convective activity on precipitation ^{18}O in isotope-enabled general circulation models. *J. Geophys. Res. Atmos.*, **123**, 13 595–13 610, https://doi.org/10.1029/2018JD029187.

IAEA, 2014: IAEA/GNIP precipitation sampling guide. International Atomic Energy Agency, 20 pp., http://www-naweb.iaea.org/napc/ih/documents/other/gnip_manual_v2.02_en_hq.pdf.

IAEA/WMO, 2021: Global Network of Isotopes in Precipitation. International Atomic Energy Agency and World Meteorological Organization, https://www.iaea.org/services/networks/gnip.

Ingraham, N. L., 1998: Isotopic variations in precipitation. *Isotope Tracers in Catchment Hydrology*, Elsevier, 87–118, https://doi.org/10.1016/B978-0-444-81546-0.50010-0.

Jiménez-Sánchez, G., P. M. Markowski, G. S. Young, and D. J. Stensrud, 2020: The Orinoco low-level jet: An investigation of its mechanisms of formation using the WRF model. *J. Geophys. Res. Atmos.*, **125**, e2020JD032810, https://doi.org/10.1029/2020JD032810.

Jones, C., 2019: Recent changes in the South America low-level jet. *NPJ Climate Atmos. Sci.*, **2**, 1–8, https://doi.org/10.1038/s41612-019-0077-5.

Kaseke, K. F., L. Wang, H. Wanke, C. Tian, and M. Lanning, 2018: Precipitation origins and key drivers of precipitation isotope (^{18}O, ^{2}H, ^{17}O) compositions over Windhoek running title: Precipitation isotopes over Windhoek. *J. Geophys. Res. Atmos.*, **123**, 7311–7330, https://doi.org/10.1029/2018JD028470.

Kattan, Z., 2019: Factors controlling stable isotopes variability in precipitation in Syria: Statistical analysis approach. *J. Earth Syst. Sci.*, **128**, 151, https://doi.org/10.1007/s12040-019-1142-5.

Kendall, L. C., and J. J. McDonnell Eds., 1999: *Isotope Tracers in Catchment Hydrology*. Elsevier, 870 pp., https://doi.org/10.1016/C2009-0-10239-8.

Kurita, N., 2013: Water isotopic variability in response to mesoscale convective system over the tropical ocean. *J. Geophys. Res. Atmos.*, **118**, 10 376–10 390, https://doi.org/10.1002/jgrd.50754.

Lawrence, M. G., 2005: The relationship between relative humidity and the dewpoint temperature in moist air: A simple conversion and applications. *Bull. Amer. Meteor. Soc.*, **86**, 225–233, https://doi.org/10.1175/BAMS-86-2-225.

Le Duy, N., I. Heidbüchel, H. Meyer, B. Merz, and H. Apel, 2018: What controls the stable isotope composition of precipitation in the Mekong Delta? A model-based statistical approach. *Hydrol. Earth Syst. Sci.*, **22**, 1239–1262, https://doi.org/10.5194/hess-22-1239-2018.

Leibundgut, C., P. Maloszewski, and C. Külls, 2009: *Tracers in Hydrology*. John Wiley & Sons, 432 pp.

Lin, D., D. P. Foster, and L. H. Ungar, 2011: VIF regression: A fast regression algorithm for large data. *J. Amer. Stat. Assoc.*, **106**, 232–247, https://doi.org/10.1198/jasa.2011.tm10113.

McDonnell, J. J., M. Bonell, M. K. Stewart, and A. J. Pearce, 1990: Deuterium variations in storm rainfall: Implications for stream hydrograph separation. *Water Resour. Res.*, **26**, 455–458, https://doi.org/10.1029/WR026i003p00455.

Montini, T. L., C. Jones, and L. M. V. Carvalho, 2019: The South American low-level jet: A new climatology, variability, and changes. *J. Geophys. Res. Atmos.*, **124**, 1200–1218, https://doi.org/10.1029/2018JD029634.

Mook, W., and K. Rozanski, 2000: *Environmental Isotopes in the Hydrological Cycle*. IAEA Publications, 39 pp.

Moriasi, D. N., J. G. Arnold, M. W. Van Liew, R. L. Bingner, R. D. Harmel, and T. L. Veith, 2007: Model evaluation guidelines for systematic quantification of accuracy in watershed simulations. *Trans. ASABE*, **50**, 885–900, https://doi.org/10.13031/2013.23153.

Mosquera, G. M., P. X. Lazo, R. Célleri, B. P. Wilcox, and P. Crespo, 2015: Runoff from tropical alpine grasslands increases with areal extent of wetlands. *Catena*, **125**, 120–128, https://doi.org/10.1016/j.catena.2014.10.010.

——, R. Célleri, P. X. Lazo, K. B. Vaché, S. S. Perakis, and P. Crespo, 2016a: Combined use of isotopic and hydrometric data to conceptualize ecohydrological processes in a high-elevation tropical ecosystem. *Hydrol. Processes*, **30**, 2930–2947, https://doi.org/10.1002/hyp.10927.

——, C. Segura, K. B. Vaché, D. Windhorst, L. Breuer, and P. Crespo, 2016b: Insights into the water mean transit time in a high-elevation tropical ecosystem. *Hydrol. Earth Syst. Sci.*, **20**, 2987–3004, https://doi.org/10.5194/hess-20-2987-2016.

Muñoz, P., R. Célleri, and J. Feyen, 2016: Effect of the resolution of tipping-bucket rain gauge and calculation method on rainfall intensities in an Andean mountain gradient. *Water*, **8**, 584, https://doi.org/10.3390/w8110534.

Nlend, B., and Coauthors, 2020: Identification of processes that control the stable isotope composition of rainwater in the humid tropical West-Central Africa. *J. Hydrol.*, **584**, 124650, https://doi.org/10.1016/j.jhydrol.2020.124650.

Noone, D., 2012: Pairing measurements of the water vapor isotope ratio with humidity to deduce atmospheric moistening and dehydration in the tropical midtroposphere. *J. Climate*, **25**, 4476–4494, https://doi.org/10.1175/JCLI-D-11-00582.1.

Orellana-Alvear, J., R. Célleri, R. Rollenbeck, and J. Bendix, 2017: Analysis of rain types and their *Z–R* relationships at different locations in the high Andes of southern Ecuador. *J. Appl. Meteor. Climatol.*, **56**, 3065–3080, https://doi.org/10.1175/JAMC-D-17-0009.1.

Padrón, R. S., B. P. Wilcox, P. Crespo, and R. Célleri, 2015: Rainfall in the Andean Páramo: New insights from high-resolution monitoring in southern Ecuador. *J. Hydrometeor.*, **16**, 985–996, https://doi.org/10.1175/JHM-D-14-0135.1.

Pang, Z., Y. Kong, K. Froehlich, T. Huang, L. Yuan, Z. Li, and F. Wang, 2011: Processes affecting isotopes in precipitation of an arid region. *Tellus*, **63B**, 352–359, https://doi.org/10.1111/j.1600-0889.2011.00532.x.

Penna, D., and Coauthors, 2012: Technical note: Evaluation of between-sample memory effects in the analysis of ^{2}H and ^{18}O of water samples measured by laser spectroscopes. *Hydrol. Earth Syst. Sci.*, **16**, 3925–3933, https://doi.org/10.5194/hess-16-3925-2012.

Picarro, 2010: ChemCorrectTM – Solving the problem of chemical contaminants in H_2O stable isotope research. White Paper 2–4, 3 pp., https://www.picarro.com/support/documents.

Poveda, G., L. Jaramillo, and L. F. Vallejo, 2014: Seasonal precipitation patterns along pathways of South American low-level jets and aerial rivers. *Water Resour. Res.*, **50**, 98–118, https://doi.org/10.1002/2013WR014087.

Putman, A. L., R. P. Fiorella, G. J. Bowen, and Z. Cai, 2019: A global perspective on local meteoric water lines: Meta-analytic insight into fundamental controls and practical constraints. *Water Resour. Res.*, **55**, 6896–6910, https://doi.org/10.1029/2019WR025181.

Rindsberger, M., M. Magaritz, I. Carmi, and D. Gilad, 1983: The relation between air mass trajectories and the water isotope composition of rain in the Mediterranean Sea area. *Geophys. Res. Lett.*, **10**, 43–46, https://doi.org/10.1029/GL010i001p00043.

Rolph, G., A. Stein, and B. Stunder, 2017: Real-time environmental applications and display sYstem: READY. *Environ. Model. Software*, **95**, 210–228, https://doi.org/10.1016/j.envsoft.2017.06.025.

Rozanski, K., and L. A. Araguas, 1995: Spatial and temporal variability of stable isotope composition of precipitation over the South American continent. *Bull. Inst. Fr. Etudes Andines*, **24**, 379–390.

Ruiz-Vásquez, M., P. A. Arias, J. A. Martínez, J. C. Espinoza, 2020: Effects of Amazon basin deforestation on regional atmospheric circulation and water vapor transport towards tropical South America. *Climate Dyn.*, **54**, 4169–4189, https://doi.org/10.1007/S00382-020-05223-4.

Sakamoto, M. S., 2011: Moisture sources and life cycle of convective systems over western Colombia. *Adv. Meteor.*, **2011**, 890759, https://doi.org/10.1155/2011/890759.

Salati, E., A. Dall'Olio, E. Matsui, and J. R. Gat, 1979: Recycling of water in the Amazon Basin: An isotopic study. *Water Resour. Res.*, **15**, 1250–1258, https://doi.org/10.1029/WR015i005p01250.

Sánchez-Murillo, R., and Coauthors, 2016: Key drivers controlling stable isotope variations in daily precipitation of Costa Rica: Caribbean Sea versus eastern Pacific Ocean

moisture sources. *Quat. Sci. Rev.*, **131**, 250–261, https://doi.org/10.1016/j.quascirev.2015.08.028.

——, A. M. Durán-Quesada, C. Birkel, G. Esquivel-Hernández, and J. Boll, 2017: Tropical precipitation anomalies and *d*-excess evolution during El Niño 2014-16. *Hydrol. Processes*, **31**, 956–967, https://doi.org/10.1002/hyp.11088.

——, and Coauthors, 2020: Tracing water sources and fluxes in a dynamic tropical environment: From observations to modeling. *Front. Earth Sci.*, **8**, 571477, https://doi.org/10.3389/feart.2020.571477.

Santhi, C., J. G. Arnold, J. R. Williams, W. A. Dugas, R. Srinivasan, and L. M. Hauck, 2001: Validation of the SWAT model on a large river basin with point and nonpoint sources. *J. Amer. Water Resour. Assoc.*, **37**, 1169–1188, https://doi.org/10.1111/j.1752-1688.2001.tb03630.x.

Singh, J., H. Knapp, and M. Demissie, 2005: Hydrologic modeling of the Iroquois River watershed using HSPF and SWAT. ISWS Contract Rep. 2004-08, Illinois State Water Survey, 343–360, http://hdl.handle.net/2142/94220.

Sloat, L. L., and Coauthors, 2018: Increasing importance of precipitation variability on global livestock grazing lands. *Nat. Climate Change*, **8**, 214–218, https://doi.org/10.1038/s41558-018-0081-5.

Stein, A. F., R. R. Draxler, G. D. Rolph, B. J. B. Stunder, M. D. Cohen, and F. Ngan, 2015: NOAA's HYSPLIT atmospheric transport and dispersion modeling system. *Bull. Amer. Meteor. Soc.*, **96**, 2059–2077, https://doi.org/10.1175/BAMS-D-14-00110.1.

Su, L., Z. Yuan, J. C. H. Fung, and A. K. H. Lau, 2015: A comparison of HYSPLIT backward trajectories generated from two GDAS datasets. *Sci. Total Environ.*, **506–507**, 527–537, https://doi.org/10.1016/j.scitotenv.2014.11.072.

Thibeault, J., A. Seth, and G. Wang, 2012: Mechanisms of summertime precipitation variability in the Bolivian Altiplano: Present and future. *Int. J. Climatol.*, **32**, 2033–2041, https://doi.org/10.1002/joc.2424.

Thies Clima, 2007: Instructions for use. Laser Precipitation Monitor 5.4110.xx.x00 V2.2xSTD, 58 pp., https://www.biral.com/wp-content/uploads/2015/01/5.4110.xx_.xxx_.pdf.

Van Der Ent, R. J., and O. A. Tuinenburg, 2017: The residence time of water in the atmosphere revisited. *Hydrol. Earth Syst. Sci.*, **21**, 779–790, https://doi.org/10.5194/hess-21-779-2017.

Van Liew, M. W., J. G. Arnold, and J. D. Garbrecht, 2003: Hydrologic simulation on agricultural watersheds: Choosing between two models. *Trans. ASAE*, **46**, 1539–1551, https://doi.org/10.13031/2013.15643.

Vera, C., and M. W. Douglas, 2006: The South American low-level jet experiment. *Bull. Amer. Meteor. Soc.*, **87**, 63–78, https://doi.org/10.1175/BAMS-87-1-63.

Vittinghoff, E., and C. E. McCulloch, 2007: Relaxing the rule of ten events per variable in logistic and cox regression. *Amer. J. Epidemiol.*, **165**, 710–718, https://doi.org/10.1093/aje/kwk052.

Vuille, M., R. S. Bradley, and F. Keimig, 2000: Climate variability in the Andes of Ecuador and its relation to tropical Pacific and Atlantic sea surface temperature anomalies. *J. Climate*, **13**, 2520–2535, https://doi.org/10.1175/1520-0442(2000)013<2520:CVITAO>2.0.CO;2.

Wang, M., and J. Paegle, 1996: Impact of analysis uncertainty upon regional atmospheric moisture flux. *J. Geophys. Res.*, **101**, 7291–7303, https://doi.org/10.1029/95JD02896.

——, J. Wright, R. Buswell, and A. Brownlee, 2013: A comparison of approaches to stepwise regression for global sensitivity analysis used with evolutionary optimization. *Proc. 13th Conf. of the Int. Building Performance Simulation Association*, Chambéry, France, International Building Performance Simulation Association, 2551–2558, http://www.ibpsa.org/proceedings/BS2013/p_1047.pdf.

Windhorst, D., T. Waltz, E. Timbe, H. G. Frede, and L. Breuer, 2013: Impact of elevation and weather patterns on the isotopic composition of precipitation in a tropical montane rainforest. *Hydrol. Earth Syst. Sci.*, **17**, 409–419, https://doi.org/10.5194/hess-17-409-2013.

Zhou, J., and K.-M. Lau, 1998: Does a monsoon climate exist over South America? *J. Climate*, **11**, 1020–1040, https://doi.org/10.1175/1520-0442(1998)011<1020:DAMCEO>2.0.CO;2.